PEER REVIEWED

The Effect of Low Temperature Range Heat Treatment on the Residual Stress of Cold Gas Dynamic Sprayed Inconel 718 Coatings via Neutron Diffraction

Sun Yung Kim[1,2] · Vladimir Luzin[3,4] · Mitchell L. Sesso[1] · John Thornton[5] · Stefan Gulizia[6]

Abstract There has been considerable interest in the application of cold gas dynamic spray (CGDS) to deposit nickel-based superalloy coatings for the repair and development of high-value components that operate under extreme environmental conditions. The CGDS process introduces residual stresses in the coating layers, but inherently effects the subsurface of the substrate in a similar manner. The present study investigates the effect of low temperature range heat treatments (100-400 °C) on the residual stress of CGDS Inconel® 718 deposited onto a presolution-treated Al7075-T651 substrate. High spatial resolution nondestructive residual stress measurements were carried out via neutron diffraction on both the CGDS deposit and substrate. The low temperature range heat treatments displayed a significant effect on both the substrate and coatings. Residual stress relaxation was exhibited in coatings that were heat-treated at the lowest temperature, whereas an increased heat treatment temperature displayed an opposite effect, increasing both the compressive residual stress in the IN718 coating and the residual tensile stress in the substrate. It is proposed the difference in thermal expansion coefficient of the two materials was the main factor responsible for the residual stresses. The effect of post-heat treatment on coating microhardness and porosity is also presented.

Keywords cold gas dynamic spray · heat treatment · neutron diffraction · nickel-based superalloy · residual stress

✉ Sun Yung Kim
SunYung.Kim@latrobe.edu.au

1   Department of Engineering, School of Engineering and Mathematical Sciences, La Trobe University, Bundoora, VIC, Australia

2   Department of Mechanical Engineering and Product Design Engineering, Swinburne University of Technology, Hawthorn, VIC, Australia

3   The Australian Centre for Neutron Scattering, Australian Nuclear Science and Technology Organisation, Lucas Heights, NSW, Australia

4   School of Engineering, The University of Newcastle, Callaghan, NSW, Australia

5   Aerospace Division, Defence Science and Technology Group, Fishermans Bend, VIC, Australia

6   Commonwealth Scientific and Industrial Research Organisation, Manufacturing Flagship, Clayton, VIC, Australia

Introduction

Nickel-based superalloys are used in a variety of applications where materials experience extreme environments, such as nuclear applications and gas turbine components for land-based power generation and aircraft jet engines.

Typically, these components operate at high temperatures and in corrosive atmospheres where they are also required to maintain mechanical integrity. The alloying constituents contained within Ni superalloys allow them to be used under such conditions since they have the ability to retain, or in some instances increase, their mechanical properties when exposed to such environments (Ref 1).

Cold gas dynamic spray (CGDS), also known as cold spray, is a relatively new thermal spray (TS) coating technique whereby particles are accelerated through the de Laval nozzle reaching supersonic velocities toward a substrate where they flatten and plastically deform to form a coating. Unlike most traditional TS techniques, cold spray is performed at relatively low gas temperatures. This reduces the negative effects that some materials experience during high-temperature deposition processes, which may result in the formation of unwanted oxides or other compositional phase changes. However, the cold spray coating formation process requires the material to undergo severe plastic deformation, which, being similar to shot peening, has been shown to induce residual stresses. The residual stress contained within and through the coating thickness is an important attribute when considering this coating technique for potential repair applications of nickel-based superalloy components (Ref 2), or as a protective coating on a dissimilar substrate material. Recent studies have shown widespread interest in cold spray deposition of nickel-based superalloy coatings.

Before cold spray was introduced, various nickel-based superalloys were deposited using a range of thermal spray and laser cladding methods. However, the high heat input required in depositing with such methods may result in undesirable effects. For instance, high-temperature TS processes produce coatings with tensile residual stresses (Ref 3-5), which, depending on the deposition conditions and final thickness, have been shown to cause delamination and limit the thickness achievable on certain shaped substrates (Ref 6, 7). These high-temperature processes can also have negative effects on the substrate by way of undesired heat treatments or forming of new phases (Ref 8-10). Furthermore, high-temperature processes, both laser and TS, that operate in normal atmospheric conditions are prone to producing deposits with high oxide content (Ref 11, 12). Although the CGDS process does not subject the feedstock to excessively high temperatures for long durations, the severe plastic deformation and localized temperatures could alter the properties of the coating.

The process by which thermal spray coatings, or thermally sprayed free forms, are fabricated, implies that they generally inherit some form of residual stress. In the as-sprayed state, the TS processes that employ and rely mostly on heat to form the coatings, such as atmospheric plasma spray (APS), are known to accumulate tensile residual stresses (Ref 13, 14). Techniques that rely on both heat and high velocities, such as high-velocity oxy-fuel (HVOF), have been shown to consist of either compressive or tensile residual stresses (Ref 15-17). Processes that rely predominately on the severe plastic deformation of the feedstock to form the deposit, such as cold spray, are reported to accumulate compressive residual stresses (Ref 18, 19). Regardless of the residual stress being compressive or tensile, either stress state will have either a positive or negative influence on the coating properties and application performance.

Residual stresses in coatings applied via high-temperature TS processes have been shown to materialize from two attributes of the deposition process (Ref 20). The first is referred to as the "deposition" stress, but is also be known as "intrinsic" or "quenching" stresses. Such stresses are the result of the splat formation process, where the molten or semi-molten particles impact the substrate and undergo quenching and rapid solidification as they cool to the substrate temperature. The second can be referred to as "thermal" stresses, which are the result of differences in thermal expansion between the coating and substrate—that will generally change simultaneously during the deposition process. Additional stresses that belong to the thermal stresses group include misfit strains in both the coatings and substrate that can develop from phase changes, structural relaxation or plastic flow (Ref 20). Thermal stresses are also greatly influenced by the coating thickness, with thicker coatings leading to greater temperature gradients in the substrate and coating system (Ref 6, 20).

The properties offered by the range of nickel-based superalloys, such as corrosion resistance and high-temperature mechanical stability, make them ideal candidates for use as coating materials, especially considering the high cost associated with fabricating and machining entire components from such materials. Moreover, provided the properties of the as-deposited superalloys are sufficient, they may also find use in certain repair operations. However, despite the range of possible applications for such materials, there remains little published work that studies the residual stress in superalloy coatings. Srinivasan et al. (Ref 21) characterized NiCr and IN625 cold-sprayed coatings deposited onto low alloy 4130 steel via various microscopy and x-ray diffraction (XRD) methods. Through-thickness residual stress was measured with a laboratory source x-ray diffractometer by removing subsequent layers followed by area measurements. The authors showed that the high compressive residual stresses in the as-sprayed coatings, in excess of 500 MPa 280 μm from the surface, could be reduced by as much as half with a 350 °C heat treatment, and heat treatment at 650 °C induced a tensile residual stress. Furthermore, the authors showed that the hardness of IN625 coatings could be

increased by 30% with heat treatments that do not exceed 650 °C, which was attributed to recrystallization of nanostructures within the spray particles. Bagherifard et al. (Ref 22) applied a similar material removal technique to determine the residual stress of cold-sprayed IN718 deposited onto aluminum alloy substrates. According to the authors, as-sprayed samples displayed negligible residual stress up to a depth of 150 μm, which is contrary to most other cold-sprayed residual stress findings.

Residual stresses in materials can be inherited at every point along a product's life cycle, from (1) the processes used to create the material, such as casting (Ref 23), (2) in any of the forming or shaping processes used to fabricate the final product (Ref 24), such as rolling, stamping and machining, and (3) during the operational life of the component, such as during temperature or loading cycles (Ref 25). These residual stresses, as the name suggests, do not alter the equilibrium condition between the components and their environment, inasmuch as they may be either beneficial or detrimental (Ref 26). For instance, surface modifications such as shot peening (Ref 27) and low plasticity burnishing (Ref 28) induce a layer of compressive residual stresses into a component surface, which is able to increase the fatigue life of superalloys in gas turbine engines that may even be exposed to foreign object damage (Ref 29). On the other hand, tensile residual stresses can be imparted during certain machining operations, especially on difficult to machine materials such as IN718 (Ref 30). These tensile residual stresses at the surface, mostly the result of localized plastic deformations and thermal effects during chip formation in machining (Ref 30-32), can promote fatigue crack growth and give rise to premature failure (Ref 32).

The residual stresses that arise in materials can be classified by the way in which they are induced, as discussed above, or depending on the scale over which they occur. As presented by a number of authors (Ref 2, 26, 33), residual stresses classified by their scale can be of three types. Type I residual stresses generally occur over large length scales, which could encompass the entire component in question. These type I residual stresses are commonly referred to as macrostresses and may arise from processes that induce large scale deformations; such as bending from external loads or warping from solidification during welding. Type II, or intergranular residual stresses, occur over the scale of the materials grain structure. These residual stresses are of special importance with polycrystalline materials, where differently orientated neighboring grains will exhibit different behaviors when subjected to mechanical or thermal loads—including phase transformations. In addition, these type II residual stresses can also be significant with those materials that contain several phases. Type III residual stresses occur on the atomic scale and are normally the result of line defects, i.e., dislocations within the structure. Both type II and type III residual stresses are considered as microstresses.

As an additional note on the residual stress review and work in this manuscript, the author is aware that residual stress is determined from the measurement of strains or displacements, rather than directly determined. However, this work uses the terms "measure" and "determine" interchangeably when referring to how the values for residual stress were obtained.

The various forms of diffraction encompass the most widely used nondestructive methods for the measurement of residual stress. However, there are other methods that rely on the materials response to various inputs to determine the residual stress, of which a brief summary of each if given by Withers (Ref 2). The use of neutrons to measure residual strain in materials was first reported by Allen et al. (Ref 34) and Pintschovius et al. (Ref 35) in 1981. The neutrons are subatomic particles with a mass similar to that of a proton, and more importantly for their use in diffraction, they carry no charge (Ref 26, 33). This enables neutrons to penetrate to significantly greater depths than any other radiation source.

The measurement of residual stress in coatings via neutron diffraction can be carried out in two configurations (Ref 36, 37) with each of them having certain advantages and drawbacks. The first configuration, referred to as horizontal scanning and used in this study, is more typical for the constant wavelength instruments based on reactor neutron sources. This configuration uses a vertically elongated gauge volume (up to 20-25 mm), while the horizontal size (i.e., spatial resolution) of the gauge volume is very tight. The practical limit of the nominal gauge volume size is 0.1 mm, while the real gauge volume is usually larger, say 0.2 mm, due to neutron beam divergency, sample misalignments, etc. Coated samples are mounted vertically and scanned horizontally. Another advantage of this configuration for stress measurements in coatings is that two principal directions, in-plane and normal, can be measured. Assuming a zero normal (perpendicular to the coating surface) stress, two unknown parameters can be resolved via two independent measurements of the two principal directions, i.e., the in-plane stress as well as the d-spacing of the material in the unstressed state (so-called d_0). A disadvantage of this method is that partial illumination can occur when measurements are done near the surface or interface. Because of that, the gauge volume can be only partially filled with the material, resulting in artificial shifts in the peak positions. These errors are also referred to as "pseudostrains" (Ref 37). In these circumstances, assuming required positioning accuracy, some correction can be made by taking two readings at the same location, orientating the sample by 180° (Ref 38).

Alternatively, especially when spatial resolution is fine, say 0.1-0.2 mm, the measurements can be made 0.1-0.2 mm away from the surface avoiding altogether the partial illumination problem. This approach is especially appropriate for coatings thicker than $\sim$ 1 mm.

The second configuration, referred to as vertical scanning (or z-scanning), is more typical for stress measurements in coatings using time-of-flight diffractometers based on the neutron spallation sources (Ref 36). In this method, the high resolution is provided in the vertical direction, while in the horizontal dimensions are much wider. A sample moves vertically within the gauge volume, scanning from the surface to the interface. This configuration results in no change in diffraction angle, hence no pseudostrains (Ref 37), and has also seen application in residual stress determination of thermal spray coatings (Ref 36). Some limitations and disadvantages of this technique are the requirement for small vertical divergency of the neutron beam, possibility of measuring only in-plane direction and, therefore, designing a procedure of dealing with d_0 and the second strain component. Additionally, the in-plane size of samples for such experiments must be limited, especially for highly attenuating materials, which might be in contradiction with having large samples sizse to avoid stress relaxation of the in-plane component on edges.

With residual stress being an important attribute of a superalloy coating, especially in applications for high-value components that must meet stringent specifications, the use of advanced techniques to analyze the residual stress can aid in promoting the use of these coatings. The literature indicates a demand to have dense deposits formed from corrosion-resistant and high-temperature, mechanically stable superalloys. Furthermore, cold spray offers an alternative to additively manufacture shapes from difficult to machine superalloys. Although much has been achieved in terms of understanding the effect of process parameters and heat treatments on the microstructure, there remains scope for further investigations into the stress states and mechanical properties of these coatings.

This study investigates the effect of a range of low temperature post-heat treatments of cold-sprayed IN718 coatings on the residual stress through the coating and substrate, which was mapped as a function of depth via neutron diffraction techniques. The relatively low heat treatment temperatures were aimed at studying the effect of substrate stress relaxation on the residual stresses in such coating–substrate systems. Microstructural properties, such as the response to Vickers microhardness indentations, coating porosity and splat/particle morphology and their correlation to pre- and post-coating processes, were characterized via scanning electron microscopy (SEM). An array of microhardness indentations were performed to

correlate the through-thickness properties of the cold-sprayed coating and substrate materials with respect to the residual stress.

Experimental Procedures

Substrate and Feedstock Materials

Inconel® 718 (IN718) feedstock powder was used as the cold spray coating material. IN718 powder was commercially available (TLS Technik GmbH, Bitterfeld, Germany) and manufactured via gas atomization. The particle morphology for the IN718 powder was spherical with a particle size distribution between + 5 to 25 μm according to the manufacturer and was used as-received. The particle size distribution analysis of the Inconel® powder was assessed with a Microtrac SRA9200 laser diffraction system (Microtrac, PA, USA). The analysis was attained from one run, with a duration of 100 s. Figure 1 shows the particle size distribution analysis for IN718, with the resulting average particle diameter of 15.13 μm. The cumulative particle size vol.% of 10, 50 and 90 are $d_{10} = 6.44$, $d_{50} = 15.13$ and $d_{90} = 29.67$ μm. Although the particle size distribution of feedstock exhibits a somewhat Gaussian profile, the IN718 powder shows an extremely wide scatter toward the larger particle diameter range, i.e., between 60 μm and 140 μm. This may be explained by two possible causes: (1) the particles were agglomerated prior to particle size analysis and were not dispersed in the analysis medium, or (2) the supplied powders contained extremely large particles due to inconsistencies in the manufacturers sieving processes.

The chemical composition of IN718 feedstock is listed in Table 1, and scanning electron microscopy (SEM) micrographs of the feedstock morphologies can be seen in Fig. 2. As it can be seen, chromium is the major alloying
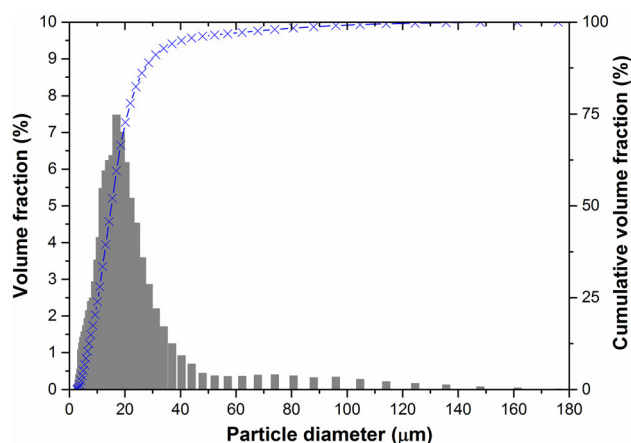

Fig. 1 Particle size distribution of IN718 feedstock

element, followed by iron. The morphology of the IN718 feedstock in Fig. 2 shows that the particles were spherical.

The substrate material was 24 mm thick Al7075-T651 plate with dimensions of 305 mm by 305 mm. The substrate surface was roughened using 600 grit SiC paper and then degreased with acetone to remove excess contaminates prior to cold spraying.

Cold Gas Dynamic Spray Condition

IN718 powders were deposited onto the Al7075-T651 substrate using a CGT KINETIKS® 4000 cold spray system (Cold Gas Technology GmbH, Ampfing, Germany), with the cold spray parameters listed in Table 2 together with a unique identifying label (ID). Optimized process parameters from earlier work (Ref 39) that used the CGT KINETIKS® 4000 cold spray system were adapted. Nitrogen was used for both the feedstock carrier gas and as the propellant used to accelerate the feedstock particles through the de Laval nozzle. The tungsten carbide TC 27 type nozzle was used and coupled with a short prechamber. Coatings were deposited at a traverse speed of 200 mm·s^{-1}.

Figure 3(a) shows the CGT KINETIKS® 4000 cold spray system setup and Fig. 3(b) a side-on close-up view of the setup used to produce samples in this study.

IN718 powders were deposited onto an Al7075-T651 substrate of dimensions 305 × 305 × 24 mm. A tungsten carbide TC 27 type nozzle equipped with a short prechamber was used, and the stand-off distance was maintained at 20 mm. The selected gas pressure and temperature initially were 3.5 MPa and 840 °C, respectively. However, after approximately 21 rasters, the nozzle became blocked. After unblocking the nozzle, the remainder of the coating, approximately 5 rasters, was produced with the same gas pressure but with a 40 °C reduction in gas temperature to reduce the likelihood of further blockages. Excessive temperatures at the throat region can lead to adhesion of heated particles on the side walls in this section of the nozzle (Ref 40). The total coating thickness produced was between 1.1 and 1.4 mm, of which approximately 0.9 mm was produced at a gas temperature of 840 °C, and the remainder at a gas temperature of 800 °C.

Table 1 The chemical composition (in wt.%) of as-received IN718 feedstock

Feedstock	Ni	Mo	Fe	Cr	Nb	Other
IN718	Bal.	3.1	17.7	18.5	5.21	< 2.0

Post-Heat Treatment on the Cold-Sprayed Samples

The cold-sprayed ID#HT sample was sectioned via electrical discharge machining (EDM) prior to post-heat treatment. Five samples were cut via EDM to dimensions of 30 × 30 × 24 mm. Four of these samples underwent individual heat treatments, and the fifth sample was retained in the 'as-sprayed' condition.

A tubular vacuum furnace with a controlled argon atmosphere was used for heat treating the four samples ID#HT-A, ID#HT-B, ID#HT-C and ID#HT-D, with the procedures listed in Table 3. The duration of the heat treatment for each sample was 100 min with the furnace ramp-up and ramp-down temperature rates of 5 and 1 °C per minute, respectively. The temperatures of heat treatment ranged from between 100 to 400 °C. It should be noted that the relatively low heat treatment temperatures were aimed at studying the effect of substrate stress relaxations on the residual stresses in such coating–substrate systems. The sample ID#HT-D underwent the highest heat treatment temperature of 400 °C, whereas ID#HT-A was heat-treated with the lowest temperature of 100 °C. Samples ID#HT-B and ID#HT-C received intermediate heat treatment temperatures of 230 and 300 °C, respectively.

Neutron Diffraction Residual Stress Measurements

Residual Stress Measurements

The neutron diffraction residual stress measurements of cold-sprayed IN718 heat-treated samples were performed on the KOWARI neutron strain scanner at the Australian Nuclear Science and Technology Organisation (ANSTO) Open Pool Australian Lightwater (OPAL) research reactor (ANSTO, Lucas Heights, Australia). Table 4 lists the selected samples for which residual stress measurements were performed via the neutron diffraction technique.
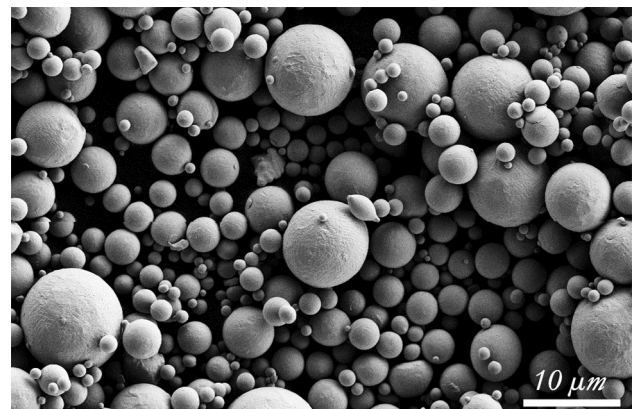

Fig. 2 SEM images of showing IN718 feedstock

Table 2 Cold spray parameters and torch used for the current study

ID	Gas pressure, MPa	Gas temperature, °C	Stand-off distance, mm	Powder feed, RPM	Rasters	Torch
ID#HT	3.5	840, 800	20	1	26	CGT 4000

ID column, the letter HT after # denotes the samples used in this study on the effect of heat treatment. Rasters are analogous to the number of layers/passes
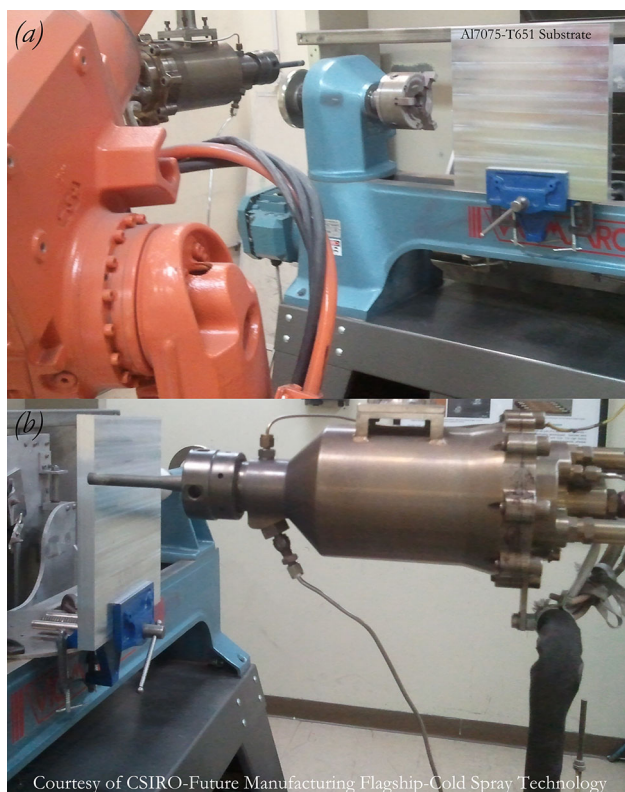

Fig. 3 CGT KINETIKS® 4000 cold spray system setup for ID#HT parameter set shown in (a) and a close-up image of the setup used to produce samples in this study (b)

Table 4 shows that residual stress measurements were carried out for cold-sprayed IN718 heat-treated samples. The samples were subjected to post-spraying heat treatment, with one sample also present as a control (ID#HT-0) that was in the 'as-sprayed' condition and originated from the same parent sample.

Images of the experimental setup can be found in Fig. 4. A range of settings related to the diffraction of the different materials were required to measure the residual stresses in the coatings and substrates. These settings consisted of gauge volume dimensions and Bragg angles for the reflections to be measured, along with monochromatic neutron beam wavelength (λ) and monochromator take-off angle ($2\theta_M$). The monochromator reflection Si(400) was used for all measurements.

Although the full details of neutron stress measurements and data analysis can be found elsewhere (Ref [41]), a short description of the experimental conditions is provided here. The $2\theta_M$ together with λ was adjusted to provide the maximum peak shift resolution and sensitivity, for a specifically chosen (hkl)-reflection that ideally should be at the optimum angle of 90 degrees, i.e., $2\theta_B \approx 90$ °. Thus, the Inconel® coating used a monochromatic beam wavelength of $\lambda = 1.5$ Å at $2\theta_M = 67$ ° that produced a scattering geometry of $2\theta_B = 90$ ° at $2\theta_M = 79$ ° for the Ni(311) reflection. The Al7075-T651 substrate employed a monochromatic beam wavelength of $\lambda = 1.73$ Å that provided a scattering geometry of $2\theta_B = 90$ ° for the Al(311) reflection.

Measured diffraction patterns for both aluminum and Inconel® were fitted with a Gaussian peak model. It is worth mentioning that the diffraction peak width was twice as large in Inconel® than in aluminum, which was evidence of a larger level of microstress in the cold-sprayed material. Due to the difference in the peak width and difference in neutron diffraction signal from aluminum and Inconel®, the measurement time was adjusted in such a way that the accuracy of measured strains was approximately 50 µ-strains. This resulted in average uncertainty for stress values in aluminum ∼ 10 MPa and ∼ 25 MPa in Inconel®.

In general, the size of the gauge volume in the through-thickness dimension, or spatial resolution of the experiment, is determined by necessity to resolve major features of the stress distribution. For the given coating–substrate system, the critical dimension that determines the spatial resolution is the coatings thickness, which was approximately above 1 mm. Thus, the gauge volume was chosen and maintained constant for both the coating and the substrate at $0.3 \times 0.3 \times 20.0$ mm^3, as per Fig. 5, therefore providing 0.3 mm through-thickness resolution. Table 5 summarizes the settings that were used for the measured coating and substrate and reflections.

In order to determine the residual stress in the coating and substrate from strain, the lattice plane d-spacing measurements were performed for two principal directions, i.e., one normal to the surface (out-of-plane) and one transverse (in-plane), as shown in Fig. 5. As mentioned earlier, cold-sprayed coatings can be considered as being in

Table 3 Heat treatment procedures for the four EDM cut samples deposited with the CGT KINETIKS® 4000 system

Sample ID	Furnace temp., °C	Duration, min	Ramp up, °C/min	Ramp down, °C/min
ID#HT-A	100	100	5	1
ID#HT-B	230	100	5	1
ID#HT-C	300	100	5	1
ID#HT-D	400	100	5	1

Table 4 List of the samples that underwent residual stress measurements via the neutron diffraction technique

Sample ID	Feedstock	Substrate	Condition
ID#HT-0	IN718	Al7075-T651	As-sprayed
ID#HT-A	IN718	Al7075-T651	Heat-treated
ID#HT-B	IN718	Al7075-T651	Heat-treated
ID#HT-C	IN718	Al7075-T651	Heat-treated
ID#HT-D	IN718	Al7075-T651	Heat-treated
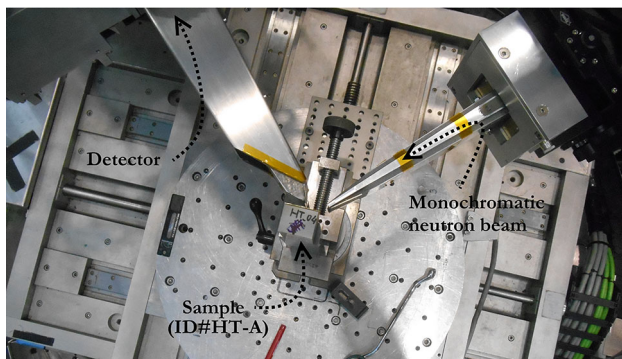
Fig. 4 Experimental setup on the KOWARI strain scanner beamline at ANSTO, showing the heat-treated samples with respect to the beam and detector set for measurement of the normal direction

a biaxial stress state with the stress in the direction normal to the surface assumed to be zero for the thin coating samples, with the procedure described in (Ref 41, 42). Under this assumption, the in-plane stress component can be calculated from the measured d-spacings using the generalized Hook's law and using diffraction elastic constants S_1 and S_2 reported in Table 5. They were calculated from the single-crystal elastic constants using the Kroner model with the help of ISODEC software (Ref 43). In these calculations, the material is assumed isotropic. Although it is known that the cold spray process can induce texture and anisotropy in the cold spray deposited materials (Ref 41), it is usually very weak to produce any significant anisotropy and in our case of relatively high deposition temperature further weakening the texture strength, the role of possible anisotropy is even less important.

The above-mentioned stress recalculating procedure does not rely on measurements of the stress-free lattice parameter (d_0). In fact, the procedure provides the d_0 profile as a by-product of the analysis.

While the assumption of zero normal stress is very accurate for a 1 mm thick coating, it is not so for the 25 mm thick substrate. However, the same approximation holds accurate enough for the first couple of millimeters and, therefore, only this first 2 mm of the substrate material below the interface was measured. For points further below the interface effective stress relaxation is expected because the sample dimensions do not support the approximation of plane stress conditions anymore, i.e., this is stress relaxation is due to an edge of the sample. The stress analysis is based on the fact considering that the substrate material plays a role of an elastic constraint for the coating and its elastic response can be approximated as local bending (linear stress profile in substrate in the first millimeters under the interface).

Microstructural Characterization

Metallographic Preparation

As-sprayed and heat-treated samples that underwent residual stress measurements were metallographically prepared for microstructural characterization. The samples were double-mounted with cold-cured epoxy resin under vacuum to prevent any undesirable delamination of the coating from the substrate and ensure proper edge retention during sectioning and polishing. The initially mounted samples were sectioned with a Secotom-50 precision cutting machine (Struers, Ballerup, Denmark). These were then vacuum-mounted for a second time to carry out grinding and polishing. Polishing was then performed using a predefined recipe for Ni-based superalloy coatings on a Tegramin-25 automated polisher (Struers, Ballerup, Denmark). The cross sections of the microstructures were examined using a Hitachi TM3030Plus (Hitachi High-Technologies Corporation, Tokyo, Japan) scanning electron microscope (SEM).

Microhardness Indentation Test

Vickers indentation test was employed to measure the microhardness of both the coatings and the coated substrates of all samples. In addition, microhardness

Fig. 5 Schematic illustration showing measurements of the transmission and reflection directions (note that measurement setup for the two directions is shown in the sample coordinate system, in which beams appears to move, while in reality the beam geometry is fixed and samples are rotated), scanning principle with step sizes of the measurements in the coating and substrate, and a principle of strain measurement through the peak shifts (greatly exaggerated, the real peak shifts are barely visible by eye)
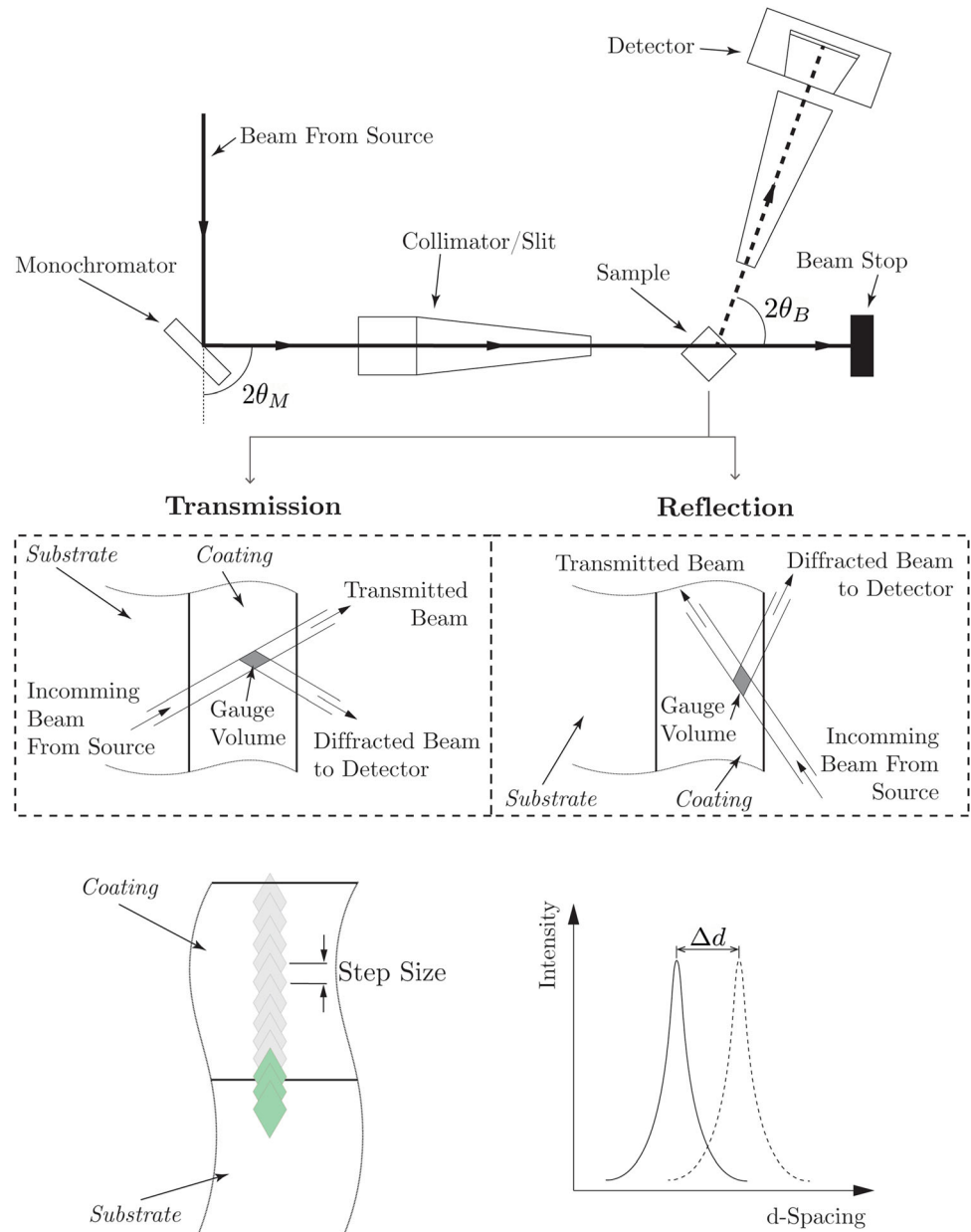
Table 5 Instrument settings and diffraction elastic constants used in the determination of the residual stresses

Reflections evaluated	$2\theta_M$, °	λ, Å	$2\theta_B$, °	Gauge volume, mm	S_1, T Pa^{-1}	$\frac{1}{2}S_2$, T Pa^{-1}
Ni (311)	67	1.5	87.6	$0.3 \times 0.3 \times 20.0$	− 1.4963	6.4157
Al (311)	79	1.73	90	$0.3 \times 0.3 \times 20.0$	− 4.9577	18.9714

measurements were taken of the bulk materials used for the coatings and substrate to determine the effect of the cold spray process. The indentation test instrument used was a DuraScan-20 G5 (Struers, Ballerup, Denmark) with an applied load of 100 g/force for a 15 s period. Microhardness measurements were taken from the top surface to the interface of the coating and from the interface to a depth of approximately 2.5 mm within the substrate. For the

coating, ten indentations per row through the thickness of the coating were obtained, while five indentations per row were measured to a depth of 2.5 mm below the interface of the substrates. In addition to this, five indentations were performed on each of the bulk materials. A minimum spacing of at least two times the average indent size was maintained between all measurements to ensure that the indent measurements did not influence each other. Figure 6

shows an example SEM image of the indentation grid used to measure the microhardness of the coating–substrate systems, and Table 6 provides details on the number of indentation tests performed for each sample.

Microhardness measurements were performed on a control set of substrates that did not undergo the coating deposition process to determine the effects of the procedure. The total number of measurements for each of the bulk material control samples, i.e., the uncoated substrates, was kept at five.

Porosity Analysis

The porosity of the cold-sprayed coatings was examined using image analysis. Ten SEM images at $300 \times$ magnification were used for the porosity analysis of each coating and the locations for each of the images were taken at random locations. All images were analyzed with ImageJ 1.48v (National Institutes of Health, Northampton, MA, USA). The $300 \times$ magnification was selected to ensure that image attributes representing porosities were clearly defined when performing the analysis. The scale and porosity characteristics were established for each image, and binary thresholding was conducted using the built-in Otsu (Ref 44) algorithm.

Results and Discussion

The Effect of Heat Treatment Temperature on the Residual Stresses

Figure 7 shows the average through-thickness residual stress profiles for IN718 coatings deposited onto 24 mm
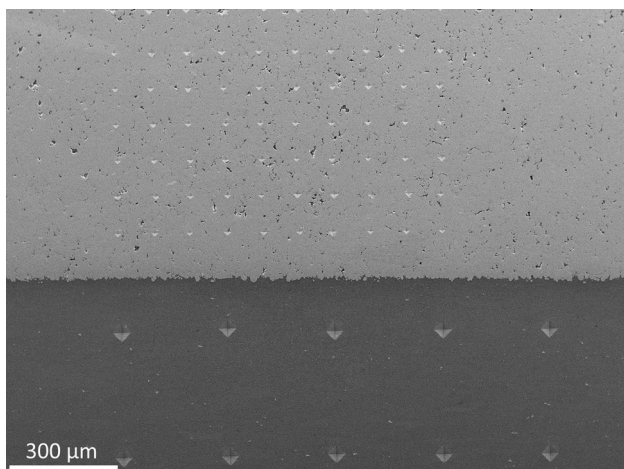

Fig. 6 SEM image of the Vickers microhardness indentation grid of the cold-sprayed IN718 coating (top) and Al7075-T651 substrate (bottom)

thick Al7075-T651, ID#HT-0 to D. The residual stress for the group of coatings plotted in Fig. 7 consists of an as-sprayed sample, and four samples that were heat-treated at 100, 230, 300 and 400 °C. Since all samples were extracted from a single coated plate, they can be considered as being identical samples that allows for a direct comparison of the measured stress profiles. The residual stress profiles of each heat-treated sample in Fig. 7(a), (b), (c) and (d) were plotted together with the reference as-sprayed sample profile in order to compare and show the variation from the initial as-sprayed sample state. Figure 7(e) displays a grouped plot to compare all samples. It can be seen, however, that even such low-temperature heat treatments have a significant effect on the magnitude of the residual stress in the IN718 coating material. Figure 7(e) demonstrates the combined effect in coating and substrate.

The residual stress in the as-sprayed IN718 coating in Fig. 7 showed much less through-thickness variation than previously reported in the authors earlier work (Ref 39) where the residual stress distribution displayed a parabolic profile within the 2.5 mm thick coating. There may be several reasons for this. First, there were slight variations in processing parameters. Second, the different residual stress profile behaviors may have been due to the substrate size and thickness onto which the coating was applied in this work. While in this study the IN718 $\sim$ 1.4 mm coating was deposited onto a $300 \times 300 \times 24$ mm plate, the IN718 2.5 mm coating from (Ref 39) was deposited on $30 \times 30 \times 12$ mm substrate; therefore, this larger substrate could dissipate heat more effectively compared to smaller coupons. Despite this, the first millimeter of the $\sim$ 2.5 mm coating stress profile also shows near-to-linear behavior, which most likely means that the parabolic stress profile occurs and develops when the coating thickness exceeds a certain critical value, this could be estimated as being $\sim$ 1 mm.

The as-sprayed stress profile can be further analyzed using the layer deposition model suggested by Tsui and Clyne (Ref 45-47) and shown in Fig. 8. The fitting of the experimental results yields numerical values of the deposition stress parameter of $- 150 \pm 20$ MPa and the thermal mismatch of $- 680 \pm 100$ μ-strain. While the first parameter characterized intrinsic stress that is induced by the cold spray process, the second parameter reflects the fact that coating and substrate materials have a different coefficient of thermal expansion (CTE) and, therefore, when spraying is finished and the sample cools off the thermally generated stresses also occur as predicted by the thermo-elasticity theory. The deposition stress value is in very good agreement with the deposition stress reported for pure nickel, $\sigma_d = - 148 \pm 10$ MPa (Ref 41). In both cases the deposition stress is compressive, which is typical for cold spray due to dominance of the peening mechanism, in

Table 6 Indentation grid details of the coating and substrate for each coating parameter

Sample ID	Indentation per row in coating	No. of columns in coating	No. of total indentations in coating	Indentation per row in substrate	No. of columns in substrate	No. of total indentations in substrate
ID#HT-0	10	10	100	5	6	30
ID#HT-A	10	10	100	5	6	30
ID#HT-B	10	10	100	5	6	30
ID#HT-C	10	10	100	5	6	30
ID#HT-D	10	10	100	5	6	30

contrast to thermal spray that usually results in a tensile quenching stress (Ref 48). Also, with a known CTE of the Al7075-T651 substrate and IN718 coating, the thermal mismatch can be transferred into the temperature drop that was ∼ 65 °C.

The model approach is also useful to check stress balance conditions as demonstrated in Fig. 8: the overall stress in the coating is compressive, which is compensated by the overall tension in the substrate. The first 0.5 mm of the substrate stress measurements are in good agreement with the model; however, for points in the substrate further below the interface, some deviation from the predicted dependence occurs as it was anticipated. It does not affect the overall stress analysis much as the stress value extrapolation to the interface is the characteristic quantity.

For the ID#HT-A sample, the application of the model approach does not result in the same good agreement, but indicates that the measured points in the substrate close to the interface are in an unsatisfactory condition. It might be a result of some measurement procedure issues or a real effect of surface local damage or impact that usually results in a compressive effect.

This type of residual stress profile is consistent with high-velocity TS processes reported in the literature. Sampath et al. (Ref 3) deposited NiAl bond coats using wire arc, plasma, HVOF and cold spray techniques. Through-thickness neutron diffraction was used to determine the stress profiles from the coating surface through to the substrate. The overall stress state of the APS coating was mostly tensile, with a change to compression at the interface, where the steel substrate interface was also in compression and changed to tensile toward the back face. A similar trend was observed for the wire arc coating of the same materials. The HVOF and cold spray coating on the other hand revealed different behaviors similar to that observed in this work, with both coatings mostly in a compressive state and the substrate going from tensile at the interface to compressive at the back face. Similar results were also displayed by Luzin et al. (Ref 4), where the authors deposited Al onto Al substrates using cold spray, HVOF and APS.

The 100 °C heat treatment on sample ID#HT-A appeared to have almost no effect on residual stresses in the substrate and coating when compared to the sample ID#HT-0 in the as-sprayed condition, as shown in Fig. 7(a). Particularly, the central portion of the ID#HT-A coating is very similar to that of the as-sprayed sample. However, at the interface and surface the residual stress of the heat-treated sample shows some slight effects of stress relaxation—though with error bars of 25-30 MPa there is no statistical certainty in this hypothesis for the interface or surface region.

The remaining samples heat-treated at 230, 300 and 400 °C (ID#HT-B–D) in Fig. 7(b), (c) and (d), however, displayed an intriguing behavior in that as the heat treatment temperature increased, the residual stress magnitude in both the coating and substrate also generally increased. The tensile residual stress observed at the interface of the substrates is between 70 MPa and 100 MPa for ID#HT-B–D as shown in the expanded plot in Fig. 7(e), balancing the effect on the coating that becomes more compressive from some −200 to −250 MPa (ID#HT-0) to some −350 to −400 MPa (ID#HT-D).

These significant variations in the residual stress state from the heat treatments could be explained by a combination of two factors related to microstructural effects of the substrate and the cold-sprayed coatings. The first are the microstructural changes that occur in Al7075-T651, an already solution-treated alloy, which can experience a significant change in material properties during additional heat treatments. The so-called retrogression and re-aging treatments (RRA) of Al7075-T651 were originally applied to these tempered alloys to increase their resistance to stress corrosion cracking without degrading their high strength (Ref 49). RRA treatments that are less than 195 °C have been shown to increase resistance to stress corrosion cracking through the grain boundary precipitates (Ref 50). However, any increase above this temperature and the Al7075-T651 displays a rapid drop in strength and hardness due to dissolution of the precipitates (Ref 49-51). In bulk materials, heat treatments above 195 °C have been
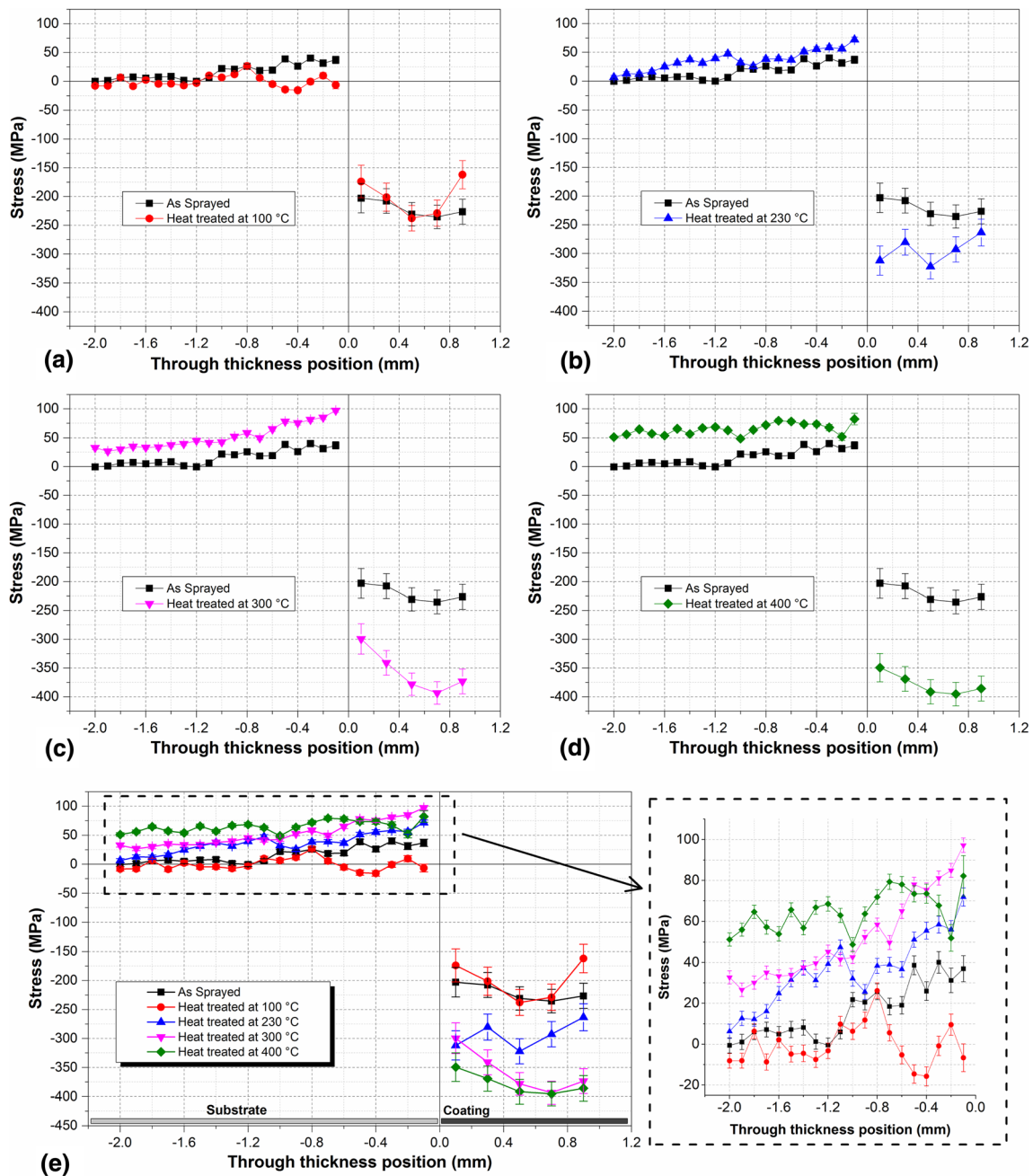
Fig. 7 The effect of post-heat treatment on the through-thickness residual stress profiles of the cold-sprayed IN718 coating onto Al7075-T651 substrate. ID#HT-A (a), ID#HT-B (b), ID#HT-C (c) and ID#HT-D (d) are all plotted with ID#HT-0. Comparison of all samples in (e). Note that where error bars are not visible, they are less than the size of the symbol

shown to reduce the residual stresses present in Al7075-T651 (Ref 52). However, this work has shown that the application of a cold-sprayed nickel-based superalloy coating increases the compressive residual stress during heat treatment, possibly due to thermal expansion mismatch and volume changes that occur during overaging of such aluminum alloys (Ref 53).

The second factor is the effect of this low range temperature heat treatment on the evolution of thermally generated stress (due to interaction of coating and substrate) in circumstances of typical cold-sprayed coating microstructure. The CTE of the two materials varies significantly, the CTE for Al7075-T651 is $\sim 23 \times 10^{-6}$, and that of IN718 is $\sim 13 \times 10^{-6}$. The thermal mismatch that
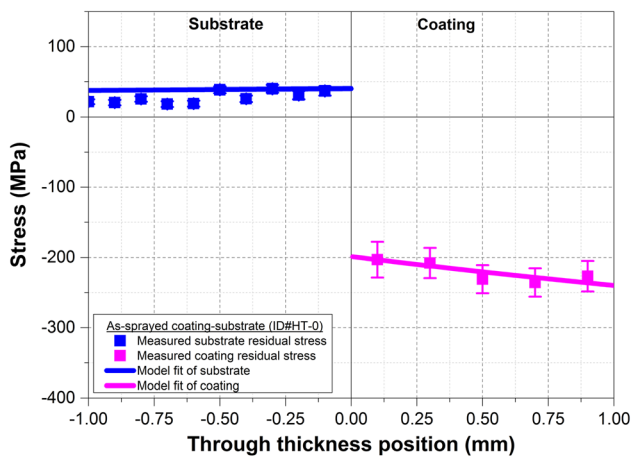
Fig. 8 The experimental residual stress profile (symbols) fitted with a model (lines) for the as-sprayed sample ID#HT-0

occurs upon heating to even such moderate temperatures, as was performed in this work, can generate significant thermal stresses. These thermal stresses, when interacting with the original residual stresses from the deposition process, can result in a stress redistribution depending on the sign and magnitude of the generated stresses and yield properties of the coating material. Furthermore, it is important to realize there will be a difference between the yield stress of the bulk and coating materials. For instance, the yield stress for solid bulk IN718 is $\sim$ 1200 MPa, yet materials formed via coating methods are not solid, they consist of a vastly different microstructure with measurable porosity as well as an inhomogeneous structure, where there is weak splat-to-splat adhesion from inconsistent bonding over the interface of each splat mixed with scattered point contacts where splats have been able to form a metallurgical bond. This is the case of those types of complex microstructures that can result in the local microstresses or stress concentrations reaching significantly higher magnitudes, at least a factor of 3 (for spherical defect) but most likely a much higher factor for crack-like defects. Therefore, average stresses of several hundreds of MPa can be translated into very high localized stresses that are comparable or exceed the yield stress of IN718. Consequently, the effective yield stress of the coating material can be much lower than that of the bulk solid material—with the exact value being a function of the microstructural details.

The same thermo-mechanical approach used above to obtain the thermal mismatch ($\Delta\varepsilon$) can be used in the opposite way to calculate the thermally generated stresses, and the results of these calculations are reported in Fig. 9. As it follows from the calculations, the heat treatment at 100 °C pertains to the overall (average) compressive stress, though less in magnitude, $-$ 50 MPa versus $-$ 220 MPa. However, the heat treatment at 230 °C and above shifts the

overall stress balance to tensile, $+$ 200, $+$ 300 and $+$ 500 MPa, for ID#HT-B, -C and -D, respectively. Taking into consideration the micromechanical setting discussed above and introducing the stress factor at least 3 or above, say 5, it is clear that even modest heat treatment of 230 °C can result in very high tensile stress concentrations of $\sim$ 1 GPa. In such circumstances the coating material is expected to yield or to develop localized microcracking in those microlocations where the tensile stress is largest. Thus, the overall effect leads to a stress relaxation to the level below the yield stress of this defect-structured material at this temperature. On return to room temperature after heat treatment, the stress level shifts the same amount in the opposite way, thus resulting in a larger magnitude compressive stress. Since the material might not be uniform and differ from layer to layer (for example, the top 6 layers are different for certain), different layers can acquire different amounts of stress relaxation on heating and a more complex than linear-like stress profile can be expected to result from heat treatment. However, much higher spatial resolution would be required to confirm this possibility.

Microstructural and Coating Properties

Figure 10 shows the data collected from the Vickers microhardness indentation measurements for as cold-sprayed and heat-treated samples as a function of depth, along with IN718 bulk hardness measurements values. The error bars in Fig. 10 represent one standard deviation. Each data point represents a mean value determined from ten measurements, i.e., $n = 10$, which range from 27 to 110 HV. These large deviations are expected when sampling in a grid pattern and being unbiased with the location of the indentation (Ref 54-56). The total number of indentations for each sample was 100 for the IN718 coating and 5 measurements on the IN718 bulk material. Figure 10(a) shows the Vickers microhardness data from the coating surface to the interface of the ID#HT-0 as-sprayed sample. As can be seen, the hardness profile does not vary significantly through the coating, and the errors associated with each row of measurements are relatively consistent. Although the mean microhardness values for all samples in Fig. 10 are less than the 5 mm thick bulk IN718, there are notable effects caused by the various heat treatments in Fig. 10(b)–(e). The 100 and 230 °C heat-treated samples in Fig. 10(b) and (c) exhibit areas in the central region of the coating where the mean microhardness dropped below 350 HV and above 400 HV at both the interface and top surface, whereas the samples heat-treated at 300 and 400 °C in Fig. 10(d) and (e) are displaying a clear increase in the overall microhardness values, with a number of the microhardness values through the thickness exceeding
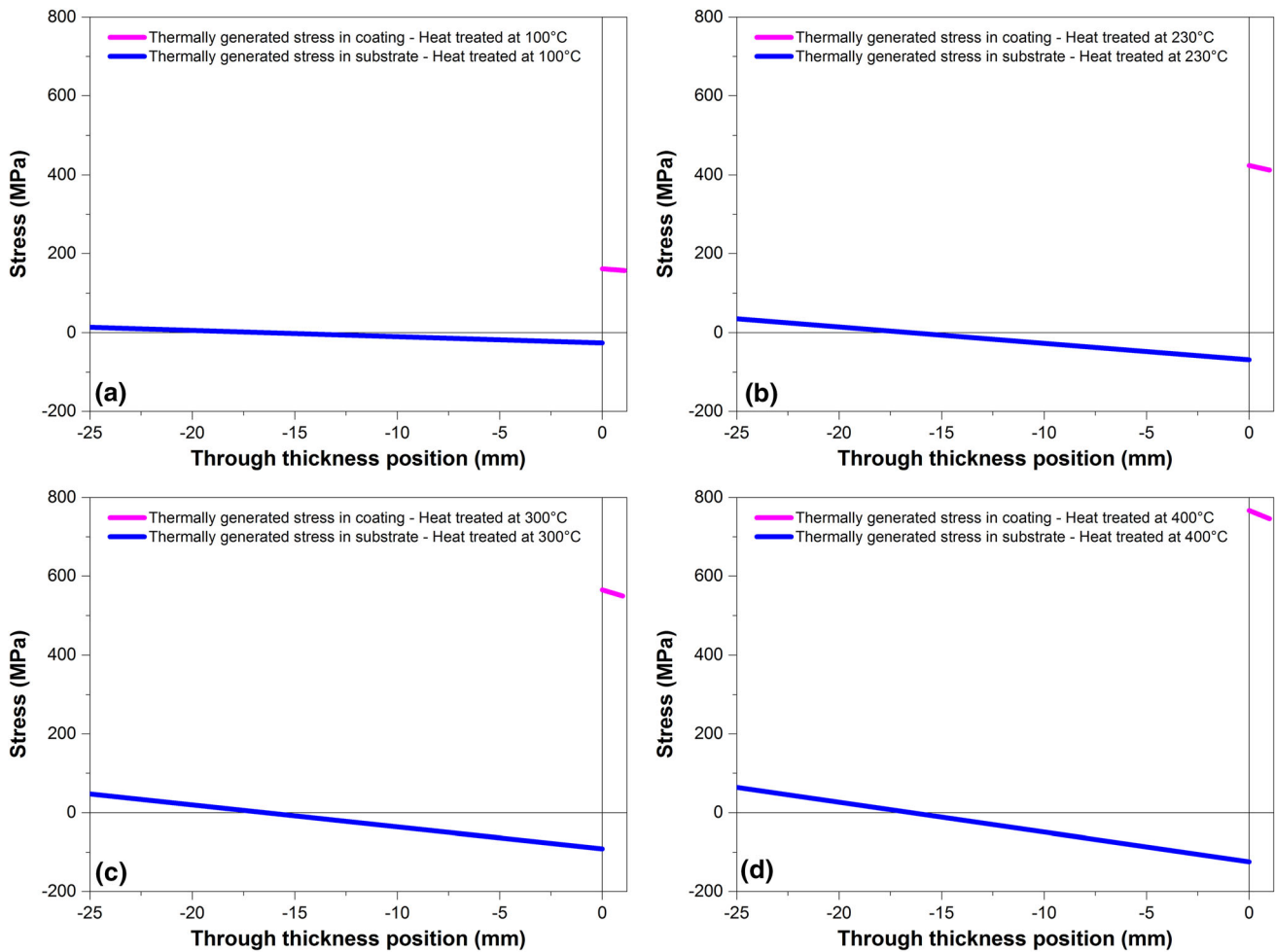
Thermo-mechanical calculation of the stress generated in the reference (as-sprayed) coating due to heat treatment. The calulated stress values are averaged over the coating thickness and rounded to tens of MPa

Sample ID	Heat Treatment Temperature [℃]	ΔT [℃]	Δε [µstrain]	Thermally Generated Stress in Coating [MPa]	Average Overall Stress in Coating [MPa]
ID# HT-0	20	0	0	0	-220
ID# HT-A	100	80	850	+170	-50
ID# HT-B	230	210	2200	+420	+200
ID# HT-C	300	280	2900	+520	+300
ID# HT-D	400	380	4000	+720	+500

Fig. 9 Calculated thermally generated stress profiles of the entire substrate coating through the thickness for various heat treatment conditions; ID#HT-A (a), ID#HT-B (b), ID#HT-C (c), ID#HT-D (d). The table summarizes the calculated data and model parameters

450 HV and 475 HV, respectively. Moreover, the 400 °C heat-treated sample displayed a number of individual microhardness values at multiple locations through the coating thickness that exceeded the mean hardness of the bulk material. There is no significant direct correlation between microhardness values and the residual stress of the coating at specific through-thickness locations, i.e., the profiles of microhardness through the thickness do not
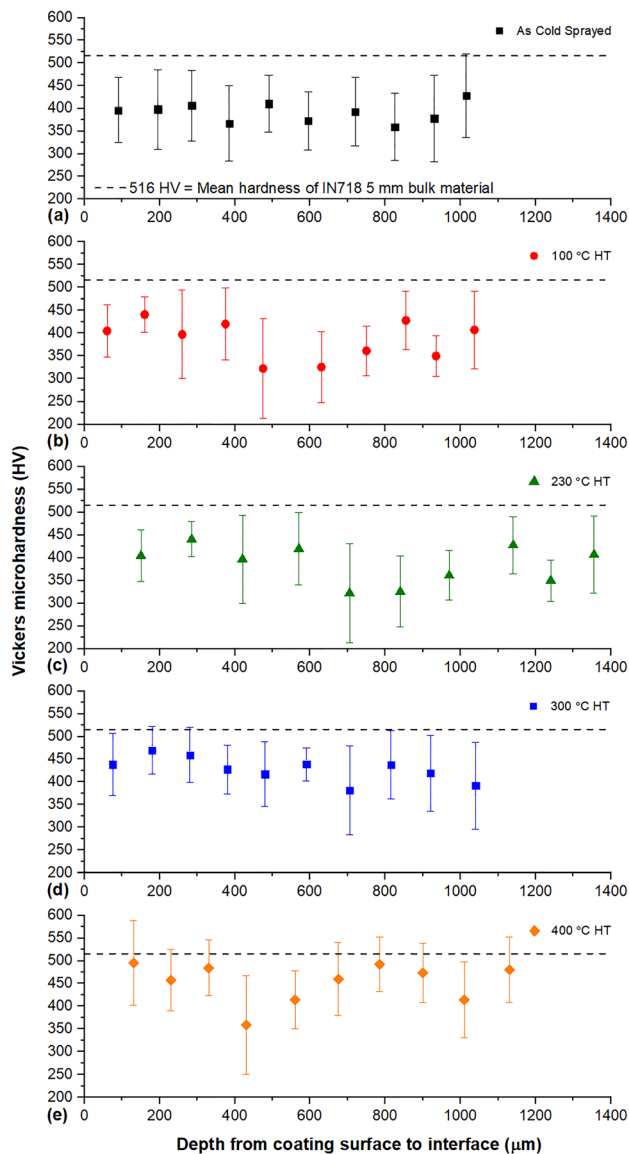
Fig. 10 Coating Vickers microhardness as a function of depth from each coating surfaces for as cold-sprayed and heat-treated samples ID#HT-0 (a), ID#HT-A (b), ID#HT-B (c), ID#HT-C (d) and ID#HT-D (e). Error bars represent one standard deviation, with $n = 10$ for each data point. The dashed line in each plot represents the mean hardness ($n = 5$) for bulk IN718 material

share a similar trend to the profiles of the individually measured residual stress points at similar locations. Partially, this might be due to a very weak stress gradient of stress through the thickness within given experimental uncertainties of stress values. However, it is observed that at higher heat treatment temperatures of 300 and 400 °C, there is an increase in the Vickers microhardness that may be related to the increased overall residual stress state in same samples. The increased coating hardness exhibited with an increasing heat treatment temperature is likely due

to the changes in residual stress rather than other temperature associated effects such as phase changes. Time–temperature-transformation diagrams for the alloy 718 (Ref 57, 58) show that no phase changes occur at temperatures below 600 °C; therefore, no precipitation hardening can be expected for the heat treatments used in this study. Contrary to that, the residual stress evolves and can impact the measured Vickers microhardness in several ways. First, for polycrystalline materials the effect of the residual macrostress on measured hardness values is well understood (Ref 59, 60) and the general principle of the relationship can be applicable here. Second, as discussed above, the change in the residual stress is due to the thermal stress cycling with localized yielding involved; therefore, there might be a degree of strain hardening that leads to the increased Vickers microhardness with heat treatment. Third, with increased macrostresses there must be a development of the microstresses (type II stress) that should also lead to the hardening of the material with the heat treatment. Albeit the relatively low temperature range of heat treatment performed in the present study for the nickel-based superalloy, there are measurable variations in hardness measurements for each 100, 230, 300 and 400 °C samples, which evidently can be related to the change in the residual stress state.

Typically, there is a relationship between coating porosity and microhardness, where higher porosity values are associated with lower microhardness (Ref 61-63). However, the current work shows a contrary relationship as a result of low temperature range heat treatment. Figure 11(a) displays the mean porosity for the as-sprayed and heat-treated samples along with mean microhardness values of each entire coating sample. Although there is a degree of error in such porosity measurements, there is a trend of the effect of heat treatments on the porosity of the coatings, where the 100 and 230 °C heat treatments result in a porosity reduction, from 4.0% in the as-sprayed condition to 3.6% and 3.7% for the two aforementioned heat treatments, respectively. A further increase in the heat treatment temperature to 300 °C resulted in an increase of 4.2% porosity, which rose further to 4.8% for the 400 °C heat treatment. Comparing this with the mean coating microhardness values also shown in Fig. 11(a), a similar, yet unexpected trend can be observed. Whether changes in porosity are the result of feedstock powder cut and/or cold spray processing parameters, other authors have shown a somewhat opposing trend. Ogawa and Niki (Ref 64) suggested the deposition of the nickel-based superalloy Inconel® 738LC (IN738LC) for rebuilding of hot section components of gas turbine engines. Although no microstructural evidence was provided, the authors showed that porosity was most affected by the processing gas pressure and temperature as well as the particle size
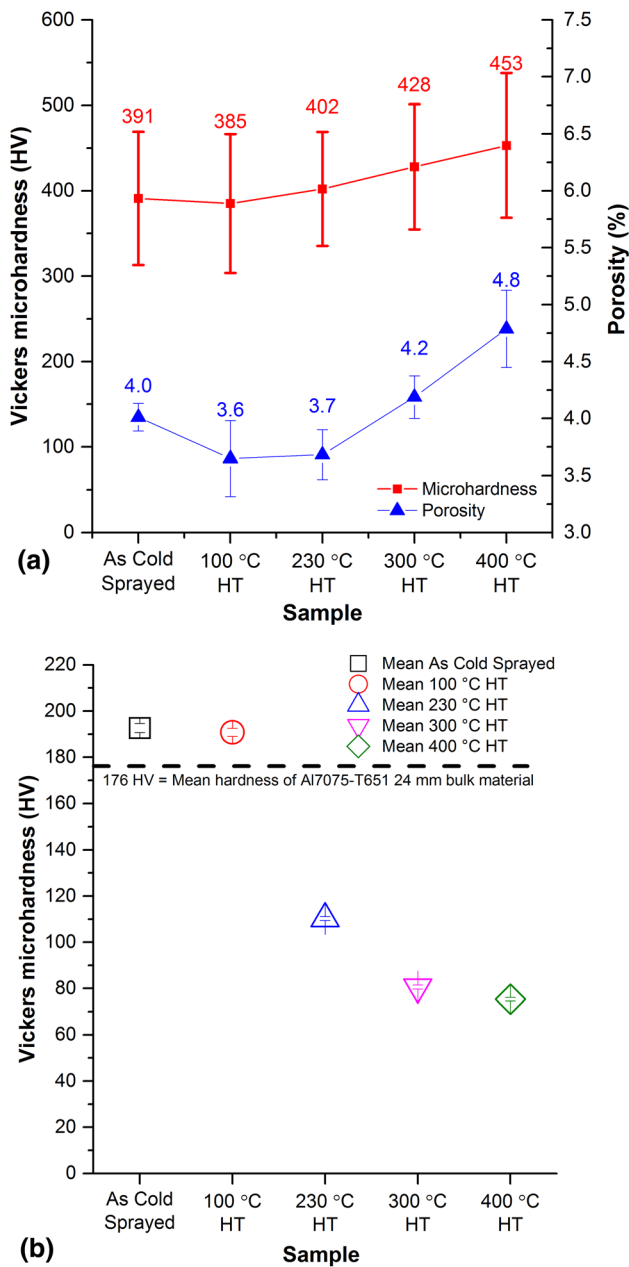
Fig. 11 Relationship between average porosity ($n = 10$) and Vickers microhardness ($n = 100$) for the IN718 coating (a), and coated substrate Vickers microhardness ($n = 30$) (b) both in the as-sprayed and in the heat-treated conditions. The dashed line in (b) represents the mean hardness ($n = 5$) for the uncoated bulk substrate material

distribution. The authors stated that specifically a smaller particle size provided a high-quality coating—which may be interpreted as a coating with low porosity and high adhesive strength, although this was not specified. The data showed that a powder cut of + 25 to 45 μm deposited at 2.5 MPa and 600 °C provided the lowest porosity of 0.38% and highest estimated adhesion strength, whereas powder cuts with small particle sizes less than 25 μm only deposited at 3.5 MPa and 800 °C resulted in the porosity of

approximately 0.97% and lower estimated adhesion strength. Overall, these results were difficult to interpret, yet showed that particle size control can play a significant role in coating quality.

An extension of the aforementioned work was later published by Ogawa and Seo (Ref 65) with more detailed analysis regarding the microstructural properties. Mechanical properties were evaluated with the use of a small punch test, details of which can be found in Ref. (Ref 66). It was found that the denser Ni-based superalloy coatings deposited with helium could be subjected to higher punch loads than coatings of higher porosity which were deposited with nitrogen. Post-heat treatment of cold-sprayed IN738LC at temperatures above 1000 °C was shown to significantly reduce the porosity of as-sprayed coatings from 4 to 2%. This heat treatment was also shown to increase the punch load energy of nitrogen-sprayed coatings almost tenfold.

Wong et al. (Ref 67, 68) cold spray formed IN718 by spraying a 6 mm thick layer onto an 80 mm diameter rotating aluminum shaft. Tensile samples were extracted from this layer via EDM and subjected to various heat treatments between 950 and 1250 °C for between 1 to 2 h. The authors found the optimum heat treatment for the IN718 to be 1 h at 1250 °C, which was found to increase the amount of metallurgical bonding between splats and decrease porosity. In addition, this heat treatment coupled with particle velocities averaging 787 ms^{-1} resulted in samples exhibiting strains of 24%, compared to the average particle velocities of 741 ms^{-1} that resulted in less ductile samples with strains of 2.2%. The work by Wong et al. (Ref 67, 68) showed that, compared to IN718 solution heat-treated sheet that has a reported strain of 12%, a range of mechanical properties were possible by controlling heat treatment and in-flight particle characteristics. Similar results for a comparable range of heat treatments were reported by Levasseur et al. (Ref 69) who observed considerable grain growth when pressureless sintering at 1250 °C was performed. In addition, it was reported that aging samples after sintering presented little effect in terms of hardness and flexural strength.

The aforementioned works presented by various authors (Ref 64-69) concluded that porosity decreases with high-temperature heat treatment range of nickel-based superalloy coatings, i.e., 950-1250 °C. However, in the current study the highest porosity and microhardness are observed at 400 °C, which is a relatively low heat treatment temperature in comparison to 950-1250 °C. On the other hand, Srinivasan et al. (Ref 21) investigated the effect of heat treatments ranging between 350-800 °C as well as dwell times on cold-sprayed IN625 coatings. Microhardness and porosity of the various heat-treated samples were compared with coatings in the as-sprayed condition. A similar trend

was observed to that in this study, in that both micro-hardness and porosity displayed an increase from the as-sprayed coating state up to a heat treatment temperature of 650 °C. Highest porosity and microhardness values were observed at the moderate heat treatment temperature of 650 °C, with microhardness significantly decreasing from 700 to 800 °C. Although a direct comparison between IN718 and IN625 coatings may be inappropriate, there are similarities on the effect of low to moderate heat treatment temperatures on nickel-based superalloy coatings. Both this work and that of Srinivasan et al. (Ref 21) have shown that cold-sprayed Inconel® coatings may undergo a number of microstructural/property changes during low–moderate-range heat treatments. An additional noteworthy difference between the works previously reported on this coating material and that of the current work is the effect of the Al7075-T651 substrate that remained attached throughout the heat treatment process—an important consideration when looking to employ cold spray as a potential repair or component improvement technique. Moreover, such coating variations need to be considered when selecting this process for applications that undergo thermal cycles or operate at elevated temperatures, which is a common use for nickel-based superalloys (Ref 70). Overall, the low range heat treatment of this coating–substrate system has resulted in measurable effects in porosity. Taking into consideration the thermo-mechanical effects of heat treatments discussed in the previous section, the increases in the porosity at the higher heat treatment temperatures above 300 °C could be the result of the localized microcracking caused by the high tensile stress concentrations. However, further investigation would be needed to confirm this.

Figure 11(b) exhibits the Vickers microhardness of the Al7075-T651 substrates for as-sprayed and four heat-treated samples, along with Al7075-T651 bulk material hardness measurement values. The samples in the as-sprayed condition and heat-treated to 100 °C display very similar substrate microhardness values of ∼ 192 HV, which is greater than the 176 HV microhardness of the Al7075-T651 bulk material. However, coated samples heat-treated at 230, 300 and 400 °C experienced a significant reduction in microhardness, with values 110, 81 and 75 HV, respectively. This reduction in microhardness of samples heat-treated above 195 °C due to the dissolution of precipitates as discussed in the previous section, which is also evident from SEM images discussed later in Fig. 12.

Although such heat treatments have resulted in changes in the residual stress states, as well as microstructural properties of the coatings and substrates, the low temperatures used have clearly affected the coating–substrate system rather than a single individual property. This highlights the importance of understanding the effect not only the application of a coating has on a substrate of a

particular material, but also how processes and post-process control can have on the resulting coating–substrate system properties.

Figure 12 displays three SEM images of each coating sample studied in this work, all imaged in backscatter electron (BSE) mode. The range of heat treatment parameters, including an as-sprayed sample, is grouped in rows as per the heading in the figure, with the first column displaying a low-magnification image of the typical sample, the second column a high-magnification image within the coating and the final column a high-magnification image of the coating–substrate interface. The SEM images in the first column in Fig. 12(a), (d), (g), (j) and (m) highlight the distribution of porosity throughout the coating for ID#HT-0, ID#HT-A, ID#HT-B, ID#HT-C and ID#HT-D, respectively.

The degree of porosity for all coatings in the first column is relatively high compared to coatings produced with feedstock sourced from the same supplier but using a different torch and somewhat different processing parameters in a previous study (Ref 39). For instance, the measured porosity for the as-sprayed coating in this study was 4.0%, whereas coatings deposited on the same substrate material in the previous study exhibited a measured porosity of 0.73% from 2.5 mm thick coatings. Both studies used the same methodology of image analysis to examine the porosity. This large variation in porosity may be due to the nozzle characteristics, which was a water-cooled glass-type nozzle, and the 2.5 times longer stand-off distance used in the previous study. Typically in thermal spray process, increasing stand-off distance would be expected to contribute to an increased porosity (Ref 71), yet the results of this study and previous works have indicated the contrary, showing that there are a number of other factors that contribute to microstructural attributes. As can be seen, extremely large particles between 50-100 μm are observed in the SEM images, which can be a locus point for delamination and poor inter-particle bonding as they may not reach the critical velocity. However, even though it is unlikely the particles reached a critical velocity that is sufficient for deposition, their presence may be due to particle entrapment within the flow stream. This clearly indicates that optimizing processing parameters with respect to a controlled particle size distributions are essential.

Comparing the various heat treatment temperatures in the first row of images, it is possible to correlate the denser microstructure for the ID#HT-A coating in Fig. 12(d) heat-treated at 100 °C, with the lowest measured porosity values in Fig. 11(a). Moreover, it can be visually observed that the porosity increases with increasing heat treatment temperature in Fig. 12(g), (j) and (m) as indicated by the increased amount of globular porosity represented by the black areas
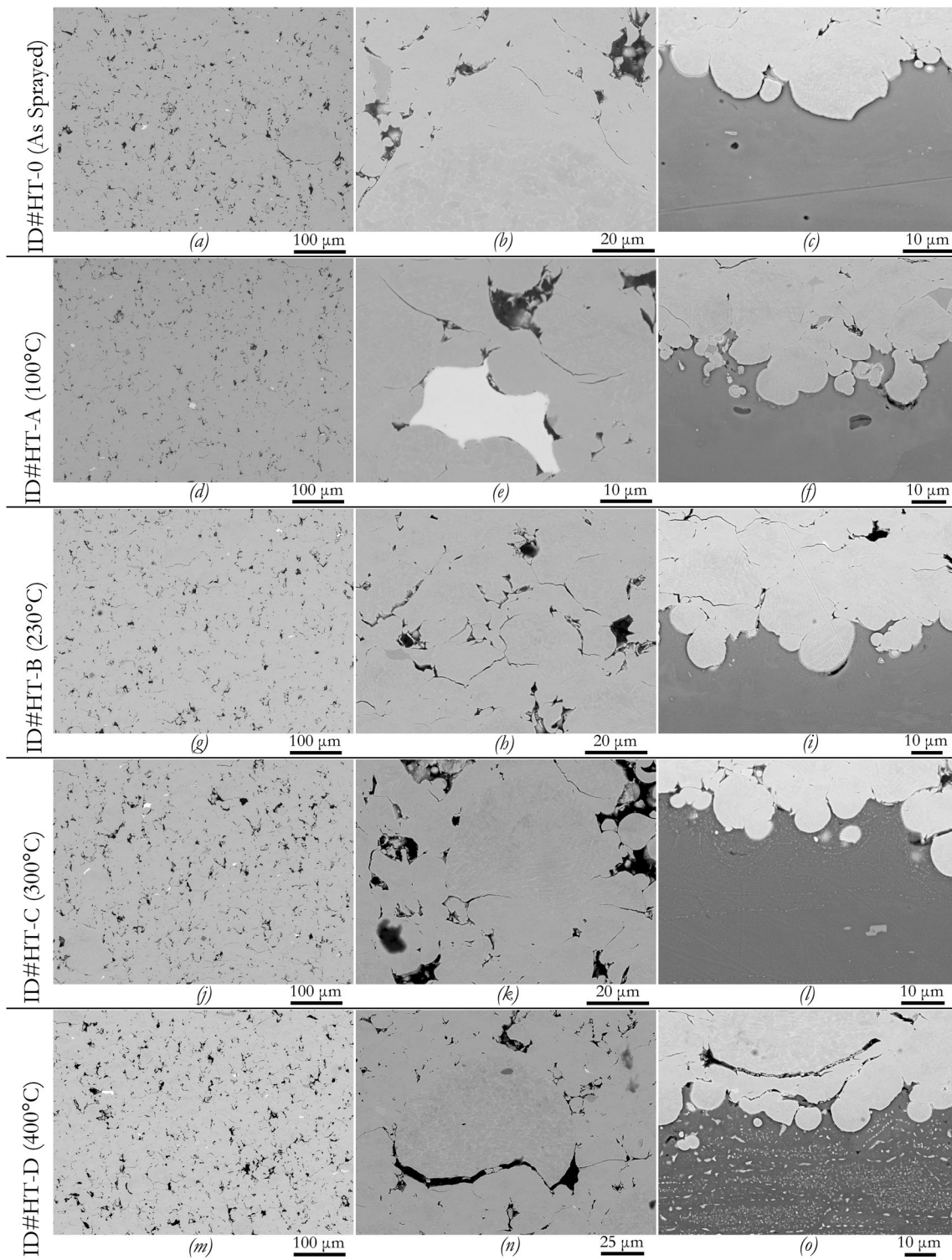
Fig. 12 SEM images of the cold-sprayed samples in this study. Each of the five rows represents the different parameter sets as per title to the left of the first column. The micrographs in the first column (a, d, g, j and m) are a representative image of the coating at low magnification, middle column (b, e, h, k and n) are a high magnification within the coating and the third column (c, f, i, l and o) are a high magnification of the interface

in the micrographs, which correlates with measured data in Fig. 11(a).

Higher-magnification images of the coating microstructures are displayed in Fig. 12(b), (e), (h), (k) and (n) for ID#HT-0, ID#HT-A, ID#HT-B, ID#HT-C and ID#HT-D, respectively. Although direct correlation of these micrographs with the residual stress, porosity and hardness in the different coatings may not be possible, it is possible to observe the various features of the microstructures that lead to the variability seen in the aforementioned measurements. The as-sprayed coating in Fig. 12(b) displays a portion of a mostly undeformed particle as can be seen from the large equiaxed crystals, above which smaller particles appear to have bonded. Other attributes such as impurities, including the light-colored niobium-rich particle in Fig. 12(e) and delamination of another oversized particle in Fig. 12(n) can also be observed.

Higher-magnification images of the coating interface are displayed in Fig. 12(c), (f), (i), (l) and (o) for ID#HT-0, ID#HT-A, ID#HT-B, ID#HT-C and ID#HT-D, respectively. Here it is possible to observe the effect of the heat treatments on the substrate material which can be correlated to the variations in residual stress. The interface of the as-sprayed and 100 °C heat-treated coating in Fig. 12(c) and (f) displays no significant visible difference. However, from the heat treatment temperature of 230 °C in Fig. 12(i), fine precipitates can be observed in the highly strained region where the IN718 particles have embedded into the substrate. Although not visible in the image, recent studies (Ref 72) have shown that shot-peened Al7075-T651 results in a high degree of recrystallization in the highly strained area, with crystal size increasing with distance from the impact zone. An increase in the heat treatment temperature to 300 °C in Fig. 12(l) has resulted in a more pronounced visibility of the precipitates as they migrate toward the grain boundaries around the fine-grained interface region.

As the heat treatment temperature was increased to 400 °C in Fig. 12(o), the precipitates in the fine-grained interface region formed into larger particles, while the coarser-grained portion of the substrate displayed a range of dispersed precipitates along the grain boundaries and finer needle-like precipitates within the larger grains. The formation of this microstructure is consistent with those observed during homogenization treatment of 7XXX alloys (Ref 73, 74), as well within heat-affected zones (HAZ) of laser clad Al7075 (Ref 75). Analysis of the 400 °C heat-treated substrate via energy-dispersive x-ray spectroscopy (EDX) revealed higher levels of magnesium and zinc, which are associated with both the grain boundary precipitate η phase ($MgZn_2/Mg_3Zn_3Al_2$) (Ref 75, 76). Residual stress studies on the HAZ of laser clad Al-7075

with visible amounts of the η phase have shown higher levels of tensile residual stress than as-received material (Ref 75), which is consistent with the stress state of the heat-treated substrate in this work.

Concluding Remarks

This work has presented a study of the effect post-heat treatments on the residual stress of cold-sprayed IN718 superalloy coatings on Al7075-T651 substrates. In addition to the residual stress the work presented the microstructural coating properties such as Vickers microhardness, of both the coating and substrates, and coating porosity.

The compressive residual stress of cold-sprayed IN718 deposited onto a presolution-treated Al7075-T651 was significantly affected by heat treatment between 230 and 400 °C. Even though the temperatures were likely not high enough to affect the stress state of the solid or cast Inconel®, the specific microstructure of the cold-sprayed material resulted in coating residual compressive stresses almost double in comparison with the as-sprayed condition, whereas heat treatment temperatures 230 °C and above increased both the coating microhardness and porosity. The increased compressive residual stress exhibited in the coatings subjected to the higher heat treatment temperatures used in this study was due to a combination of microstructural changes in the substrate as well as the evolution of the thermally generated stresses (due to differences in the thermal expansion of the coating and substrate materials) upon thermal cycling during heat treatment. The lowest heat treatment temperature also resulted in a decrease of the coating porosity and microhardness compared to the as-sprayed condition. At higher heat treatment temperatures, the increased compressive residual stress and effects related to it (strain hardening and microstress) were observed to increase the microhardness, whereas the increase in porosity at these high heat treatment temperatures may have been due to microcracking caused by the high tensile stress concentrations within the coatings microstructure during heat treatment. While this increase in porosity could potentially lead to a decrease in microhardness, the stress effects apparently were greater so that the overall effect was due to residual stresses.

As an outcome of this study, it is noteworthy to remark application environments may expose either the substrate or coating material to conditions that may alter the physical properties—such as the case in this work, where the two materials display a substantial thermal mismatch during low temperature range heat treatments. Furthermore, this behavior indicates that prior knowledge of the substrate and coating properties and monitoring the temperature of heat-sensitive substrates in service may be needed to

control the residual stress state within cold-sprayed coatings. Moreover, the results show that careful consideration and matching of the substrate and coating properties need to be taken prior to depositing materials that retain their thermo-mechanical properties at high temperatures and strain rates such as nickel-based superalloys.

References

1. R.C. Reed, *The Superalloys: Fundamentals and Applications*, Cambridge University Press, Cambridge, 2006
2. P.J. Withers, Residual Stress and Its Role in Failure, *Rep. Prog. Phys.*, 2007, **70**(12), p 2211-2264
3. S. Sampath, X.Y. Jiang, J. Matejicek, L. Prchlik, A. Kulkarni, and A. Vaidya, Role of Thermal Spray Processing Method on the Microstructure, Residual Stress and Properties of Coatings: An Integrated Study for Ni-5 Wt%Al Bond Coats, *Mater. Sci. Eng. A*, 2004, **364**(1–2), p 216-231
4. V. Luzin, A. Valarezo, and S. Sampath, Through-Thickness Residual Stress Measurement in Metal and Ceramic Spray Coatings by Neutron Diffraction, *Mater. Sci. Forum*, 2008, **571–572**, p 315-320
5. V. Luzin, H.-J. Prask, T. Gnaupel-Herold, and S. Sampath, Use of Neutron Diffraction for Stress Measurements in Thin and Thick Thermal Sprayed Coatings, *Int. Heat Treat. Surf. Eng.*, 2010, **4**(1), p 17-24
6. J. Matejicek, S. Sampath, P.C. Brand, and H.J. Prask, Quenching, Thermal and Residual Stress in Plasma Sprayed Deposits: NiCrAlY and YSZ Coatings, *Acta Mater.*, 1999, **47**(2), p 607-617
7. S.J. Howard, Y.C. Tsui, and T.W. Clyne, The Effect of Residual Stresses on the Debonding of Coatings—I. A Model for Delamination at a Bimaterial Interface, *Acta Metall. Mater.*, 1994, **42**(8), p 2823-2836
8. P. Chraska, J. Dubsky, B. Kolman, J. Llavsky, and J. Forman, Study of Phase Changes in Plasma Sprayed Deposits, *J. Therm. Spray Technol.*, 1992, **1**(4), p 301-306
9. H.G. Chun, T.Y. Cho, J.H. Yoon, and G.H. Lee, Improvement of Surface Properties of Inconel718 by HVOF Coating with WC-Metal Powder and by Laser Heat Treatment of the Coating, *Adv. Mater. Sci. Eng.*, 2015, **2015**, p e468120
10. A. Babilius, *Influence of Temperature on the Phases Changes of HVOF Sprayed Tungsten Carbide Coatings* (Kaunas University of Technology, Lithuania, 2003). http://www.matsc.ktu.lt/index.php/MatSc/article/view/26701
11. J.R. Davis, *Handbook of Thermal Spray Technology*, ASM International, Philadelphia, 2004
12. P.L. Fauchais, J.V.R. Heberlein, and M.I. Boulos, Overview of Thermal Spray, *Thermal Spray Fundamentals*, P.L. Fauchais, J.V.R. Heberlein, and M.I. Boulos, Ed., Springer, Boston, 2014, p 17-72
13. Y.C. Tsui, C. Doyle, and T.W. Clyne, Plasma Sprayed Hydroxyapatite Coatings on Titanium Substrates Part 1: Mechanical Properties and Residual Stress Levels, *Biomaterials*, 1998, **19**(22), p 2015-2029
14. J. Matejíček, S. Sampath, and J. Dubsky, X-ray Residual Stress Measurement in Metallic and Ceramic Plasma Sprayed Coatings, *J. Therm. Spray Technol.*, 1998, **7**(4), p 489-496
15. A.M. Venter, T. Pirling, T. Buslaps, O.P. Oladijo, A. Steuwer, T.P. Ntsoane, L.A. Cornish, and N. Sacks, Systematic Investigation of Residual Strains Associated with WC–Co Coatings Thermal Sprayed onto Metal Substrates, *Surf. Coat. Technol.*, 2012, **206**(19–20), p 4011-4020
16. J. Stokes and L. Looney, Residual Stress in HVOF Thermally Sprayed Thick Deposits, *Surf. Coat. Technol.*, 2004, **177–178**, p 18-23
17. C.R.C. Lima, J. Nin, and J.M. Guilemany, Evaluation of Residual Stresses of Thermal Barrier Coatings with HVOF Thermally Sprayed Bond Coats Using the Modified Layer Removal Method (MLRM), *Surf. Coat. Technol.*, 2006, **200**(20–21), p 5963-5972
18. V. Luzin, K. Spencer, and M.-X. Zhang, Residual Stress and Thermo-Mechanical Properties of Cold Spray Metal Coatings, *Acta Mater.*, 2011, **59**(3), p 1259-1270
19. K. Spencer, V. Luzin, N. Matthews, and M.-X. Zhang, Residual Stresses in Cold Spray Al Coatings: The Effect of Alloying and of Process Parameters, *Surf. Coat. Technol.*, 2012, **206**(19–20), p 4249-4255
20. T.W. Clyne and S.C. Gill, Residual Stresses in Thermal Spray Coatings and Their Effect on Interfacial Adhesion: A Review of Recent Work, *J. Therm. Spray Technol.*, 1996, **5**(4), p 401
21. D. Srinivasan, V. Chandrasekhar, R. Amuthan, Y.C. Lau, and E. Calla, Characterization of Cold-Sprayed IN625 and NiCr Coatings, *J. Therm. Spray Technol.*, 2016, **25**(4), p 725-744
22. S. Bagherifard, G. Roscioli, M.V. Zuccoli, M. Hadi, G. D'Elia, A.G. Demir, B. Previtali, J. Kondás, and M. Guagliano, Cold Spray Deposition of Freestanding Inconel Samples and Comparative Analysis with Selective Laser Melting, *J. Therm. Spray Technol.*, 2017, **26**(7), p 1517-1526
23. E.M. Johnson, T.R. Watkins, J.E. Schmidlin, and S.A. Dutler, A Benchmark Study on Casting Residual Stress, *Metall. Mater. Trans. A*, 2012, **43**(5), p 1487-1496
24. T. Berruti, M. Lavella, and M.M. Gola, Residual Stresses on Inconel 718 Turbine Shaft Samples After Turning, *Mach. Sci. Technol.*, 2009, **13**(4), p 543-560
25. B.J. Foss, S. Gray, M.C. Hardy, S. Stekovic, D.S. McPhail, and B.A. Shollock, Analysis of Shot-Peening and Residual Stress Relaxation in the Nickel-Based Superalloy RR1000, *Acta Mater.*, 2013, **61**(7), p 2548-2559
26. P.J. Withers and H.K.D.H. Bhadeshia, Residual Stress Part 1—Measurement Techniques, *Mater. Sci. Technol.*, 2001, **17**(4), p 355-365
27. R.L. Mattson and J.G. Roberts, *The Effect of Residual Stresses Induced by Strain-Peening Upon Fatigue Strength*, vol. 68 (SAE International, SAE Transactions, Warrendale, 1960), pp. 130–136. https://www.jstor.org/stable/44565121?seq=1#metadata_info_tab_contents
28. P. Prevéy, J. Telesman, T. Gabb, and P. Kantzos, FOD Resistance and Fatigue Crack Arrest in Low Plasticity Burnished IN718, in *Proceedings of the 5th National Turbine Engineering HCF Conference*, (Chandler, AZ)
29. P. Prevéy, The Effect of Cold Work on the Thermal Stability of Residual Compression in Surface Enhanced IN718, in *HeatTreating 2000: Proceedings of the 20th Conference* (ASM International, Materials Park), p 426–434
30. R.M. Arunachalam, M.A. Mannan, and A.C. Spowage, Residual Stress and Surface Roughness When Facing Age Hardened Inconel 718 with CBN and Ceramic Cutting Tools, *Int. J. Mach. Tools Manuf.*, 2004, **44**(9), p 879-887
31. R. M'Saoubi, D. Axinte, C. Herbert, M. Hardy, and P. Salmon, Surface Integrity of Nickel-Based Alloys Subjected to Severe

Plastic Deformation by Abusive Drilling, *CIRP Ann.*, 2014, **63**(1), p 61-64

32. E. Brinksmeier and H.K. Tönshoff, X-ray Stress Measurement—A Tool for the Study and Layout of Machining Processes, *CIRP Ann. Manuf. Technol.*, 1985, **34**(1), p 485-490

33. I.C. Noyan and J.B. Cohen, *Residual Stress: Measurement by Diffraction and Interpretation*, Springer, New York, 1987

34. A. Allen, C. Andreani, M.T. Hutchings, and C.G. Windsor, Measurement of Internal Stress within Bulk Materials Using Neutron Diffraction, *NDT Int.*, 1981, **14**(5), p 249-254

35. L. Pintschovius, V. Jung, E. Macherauch, R. Schäfer, and O. Vöhringer, Determination of Residual Stress Distributions in the Interior of Technical Parts by Means of Neutron Diffraction, *Residual Stress and Stress Relaxation*, E. Kula and V. Weiss, Ed., Springer, Berlin, 1982, p 467-482

36. R. Ahmed, H. Yu, S. Stewart, L. Edwards, and J.R. Santisteban, Residual Strain Measurements in Thermal Spray Cermet Coatings via Neutron Diffraction, *J. Tribol.*, 2007, **129**(2), p 411-418

37. M.E. Fitzpatrick and A. Lodini, *Analysis of Residual Stress by Diffraction Using Neutron and Synchrotron Radiation*, Taylor & Francis, London, 2003

38. V. Luzin, A. Vackel, A. Valarezo, and S. Sampath, Neutron Through-Thickness Stress Measurements in Coatings with High Spatial Resolution, *Mater. Sci. Forum*, 2017, **905**, p 165-173

39. S.Y. Kim, *Residual Stress and Finite Element Analysis of Cold Gas Dynamic Sprayed Nickel Based Superalloys*. Ph.D. Thesis, Swinburne University of Technology, 2017

40. X. Wang, B. Zhang, J. Lv, and S. Yin, Investigation on the Clogging Behavior and Additional Wall Cooling for the Axial-Injection Cold Spray Nozzle, *J. Therm. Spray Technol.*, 2015, **24**(4), p 696-701

41. V. Luzin, K. Spencer, M. Zhang, N. Matthews, J. Davis, and M. Saleh, Residual Stresses in Cold Spray Coatings, *Cold-Spray Coatings*, P. Cavaliere, Ed., Springer, Cham, 2018, p 451-480

42. W.B. Choi, L. Li, V. Luzin, R. Neiser, T. Gnäupel-Herold, H.J. Prask, S. Sampath, and A. Gouldstone, Integrated Characterization of Cold Sprayed Aluminum Coatings, *Acta Mater.*, 2007, **55**(3), p 857-866

43. T. Gnäupel-Herold, ISODEC: Software for Calculating Diffraction Elastic Constants, *J. Appl. Crystallogr.*, 2012, **45**(3), p 573-574

44. N. Otsu, A Threshold Selection Method from Gray-Level Histograms, *IEEE Trans. Syst. Man Cybern.*, 1979, **9**(1), p 62-66

45. Y.C. Tsui and T.W. Clyne, An Analytical Model for Predicting Residual Stresses in Progressively Deposited Coatings Part 1: Planar Geometry, *Thin Solid Films*, 1997, **306**(1), p 23-33

46. Y.C. Tsui and T.W. Clyne, An Analytical Model for Predicting Residual Stresses in Progressively Deposited Coatings Part 2: Cylindrical Geometry, *Thin Solid Films*, 1997, **306**(1), p 34-51

47. Y.C. Tsui and T.W. Clyne, An Analytical Model for Predicting Residual Stresses in Progressively Deposited Coatings Part 3: Further Development and Applications, *Thin Solid Films*, 1997, **306**(1), p 52-61

48. J. Pina, A. Dias, and J.L. Lebrun, Study by X-ray Diffraction and Mechanical Analysis of the Residual Stress Generation during Thermal Spraying, *Mater. Sci. Eng. A*, 2003, **347**(1), p 21-31

49. *C.B. Reducing the Susceptibility of Alloys, Particularly Aluminium Alloys, to Stress Corrosion Cracking*, U.S. Patent 3,856,584 A, 1974

50. J.K. Park and A.J. Ardell, Effect of Retrogression and Reaging Treatments on the Microstructure of AL-7075-T651, *Metall. Trans. A*, 1984, **15**(8), p 1531-1543

51. J.M. Papazian, The Effects of Warm Working on Aluminum Alloy 7075-T651, *Mater. Sci. Eng.*, 1981, **51**(2), p 223-230

52. M.S. Younger and K.H. Eckelmeyer, *Overcoming Residual Stresses and Machining Distortion in the Production of Aluminum Alloy Satellite Boxes* (Sandia National Laboratories, United States, 2007). https://www.osti.gov/biblio/922073/

53. R.T. Holt, R. Wallace, W. Wallace, and D.L. DuQuesnay, *RRA Heat Treatment of Large Al 7075-T6 Components* (NATO, 2000). https://apps.dtic.mil/sti/citations/ADP010412

54. C.K. Lin and C.C. Berndt, Statistical Analysis of Microhardness Variations in Thermal Spray Coatings, *J. Mater. Sci.*, 1995, **30**(1), p 111-117

55. T. Valente, Statistical Evaluation of Vicker's Indentation Test Results for Thermally Sprayed Materials, *Surf. Coat. Technol.*, 1997, **90**(1–2), p 14-20

56. M. Factor and I. Roman, Vickers Microindentation of WC–12%Co Thermal Spray Coating: Part 1: Statistical Analysis of Microhardness Data, *Surf. Coat. Technol.*, 2000, **132**(2–3), p 181-193

57. D.D. Keiser and H.L. Brown, *Review of the Physical Metallurgy of Alloy 718*, ANCR–1292, 1976

58. A. Oradei-Basile and J.F. Radavich, A Current T–T–T Diagram for Wrought Alloy 718, in *Superalloys 718, 625 and Various Derivatives (1991)*, 1991 TMS, 1991, p 325–335

59. S. Carlsson and P.-L. Larsson, On the Determination of Residual Stress and Strain Fields by Sharp Indentation Testing. Part I: Theoretical and Numerical Analysis, *Acta Mater.*, 2001, **49**(12), p 2179-2191

60. S. Suresh and A.E. Giannakopoulos, A New Method for Estimating Residual Stresses by Instrumented Sharp Indentation, *Acta Mater.*, 1998, **46**(16), p 5755-5767

61. P. Sudharshan Phani, D. Srinivasa Rao, S.V. Joshi, and G. Sundararajan, Effect of Process Parameters and Heat Treatments on Properties of Cold Sprayed Copper Coatings, *J. Therm. Spray Technol.*, 2007, **16**(3), p 425-434

62. B. AL-Mangour, P. Vo, R. Mongrain, E. Irissou, and S. Yue, Effect of Heat Treatment on the Microstructure and Mechanical Properties of Stainless Steel 316L Coatings Produced by Cold Spray for Biomedical Applications, *J. Therm. Spray Technol.*, 2014, **23**(4), p 641-652

63. S.H. Zahiri, C.I. Antonio, and M. Jahedi, Elimination of Porosity in Directly Fabricated Titanium via Cold Gas Dynamic Spraying, *J. Mater. Process. Technol.*, 2009, **209**(2), p 922-929

64. K. Ogawa and T. Niki, Repairing of Degraded Hot Section Parts of Gas Turbines by Cold Spraying, *Key Eng. Mater.*, 2009, **417–418**, p 545-548

65. K. Ogawa and D. Seo, Repair of Turbine Blades Using Cold Spray Technique, *Advances in Gas Turbine Technology*, E. Benini, Ed., InTech, London, 2011,

66. J.-M. Baik, J. Kameda, and O. Buck, Small Punch Test Evaluation of Intergranular Embrittlement of an Alloy Steel, *Scr. Metall.*, 1983, **17**(12), p 1443-1447

67. W. Wong, E. Irissou, J.-G. Legoux, F. Bernier, P. Vo, S. Yue, S. Michiyoshi, and H. Fukanuma, Cold Spray Forming of Inconel 718, Thermal Spray 2012, in *Proceedings of the International Thermal Spray Conference, May 2012 (Houston, Texas USA)*, ASM International, Materials Park, 2012, p 243–248

68. W. Wong, E. Irissou, P. Vo, M. Sone, F. Bernier, J.-G. Legoux, H. Fukanuma, and S. Yue, Cold Spray Forming of Inconel 718, *J. Therm. Spray Technol.*, 2013, **22**(2–3), p 413-421

69. D. Levasseur, S. Yue, and M. Brochu, Pressureless Sintering of Cold Sprayed Inconel 718 Deposit, *Mater. Sci. Eng. A*, 2012, **556**, p 343-350

70. M. Okazaki, High-Temperature Strength of Ni-Base Superalloy Coatings, *Sci. Technol. Adv. Mater.*, 2001, **2**(2), p 357-366

71. J. Henao, A. Concustell, I.G. Cano, N. Cinca, S. Dosta, and J.M. Guilemany, Influence of Cold Gas Spray Process Conditions on the Microstructure of Fe-Based Amorphous Coatings, *J. Alloys Compd.*, 2015, **622**, p 995-999

72. S. Singh, Y. Guo, B. Winiarski, T.L. Burnett, P.J. Withers, and M. De Graef, High Resolution Low KV EBSD of Heavily Deformed and Nanocrystalline Aluminium by Dictionary-Based Indexing, *Sci. Rep.*, 2018, **8**(1), p 10991

73. J. Waldman, H. Sulinski, and H. Markus, The Effect of Ingot Processing Treatments on the Grain Size and Properties of Al Alloy 7075, *Metall. Trans.*, 1974, **5**(3), p 573-584

74. J.-L. Fu, H.-J. Jiang, and K.-K. Wang, Influence of Processing Parameters on Microstructural Evolution and Tensile Properties for 7075 Al Alloy Prepared by an ECAP-Based SIMA Process, *Acta Metall. Sin. Engl. Lett.*, 2018, **31**(4), p 337-350

75. R. Cottam, V. Luzin, Q. Liu, Y.C. Wong, J. Wang, and M. Brandt, Investigation into Heat Treatment and Residual Stress in Laser Clad AA7075 Powder on AA7075 Substrate, *Metallogr. Microstruct. Anal.*, 2013, **2**(4), p 205-212

76. J.-Q. Su, T.W. Nelson, R. Mishra, and M. Mahoney, Microstructural Investigation of Friction Stir Welded 7050-T651 Aluminium, *Acta Mater.*, 2003, **51**(3), p 713-729

Publisher's Note Springer Nature remains neutral with regard to jurisdictional claims in published maps and institutional affiliations.